Position Estimation for Self-Sensing Magnetic Bearings Based on Double Detection of Current Slopes

Jinou Wang, Andreas Binder

Technische Universität Darmstadt, Institute of Electrical Energy Conversion, Landgraf-Georg-Str. 4, 64283 Darmstadt, Germany, jwang@ew.tu-darmstadt.de, abinder@ew.tu-darmstadt.de

***Abstract*—This paper introduces a new approach to estimate the rotor position of self-sensing magnetic bearings, which works on detecting the current slopes during both positive and negative voltage switching of PWM amplifiers. The position is estimated using the current slopes straightforward. The consideration of double current slopes shows advantages concerning the reduction of the influences of the coil resistance and the induced voltage due to the rotor movement. The current slope is calculated by multiple current sampling, therefore, no additional hardware is needed for the current slope measurement. Experimental results verified the proposed approach.**

I. INTRODUCTION

Self-sensing magnetic bearing technology has been researched intensively since the last decades. Although commercial applications already exist [1], [2], there are still technical challenges concerning the improvements of dynamic and linearity of the position estimation. These two factors are very important for a fast and accurate position control.

The modern self-sensing techniques all seem to use a kind of high-frequency interrogation signal for position estimation [3-6]. To avoid the hardware signal-injection unit, the switching ripple, which is a nature of PWM power amplifiers, is most applied. The reason is that the switched voltage as an interrogation signal has the highest frequency and amplitude, which should deliver the best estimation performance. But due to the position control, the duty cycle of the switched voltage varies, which leads to considerable decrease of the achievable performance. Many experts have worked on this issue in the past years [3, 5].

The above approaches model the triangle current ripple waveform with a set of sinusoidal harmonics and consider the position estimation in the linear periodic point of view. Due to the nature of the inductance, high frequency harmonics have more amplitude deviations with the same inductance change caused by the rotor movement, and therefore make much more contribution to the SNR (signal-to-noise ratio) and to the dynamic of the position estimation. But the estimator based on the above modelling cannot handle all frequencies, especially in the high frequency region. Therefore, the current ripple is theoretically not fully utilized for the position estimation.

To fully exploit the current ripple, it seems better to model it directly with triangle signals. Then, the current slopes will be used, as first introduced in [7]. This perspective looks directly at the nature of the current response of electromagnets

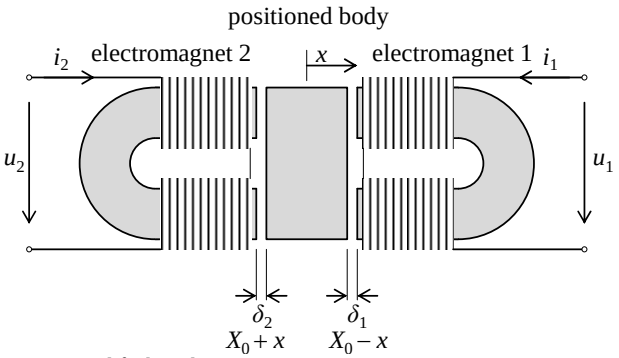

Fig. 1: A simplified single-axis actuator

driven by switched voltages. In [7], the rotor position is sensorless controlled, but there is no explicit position output, therefore, the position control and the position estimation are not decoupled. Independent position estimation makes the design of the position controller more flexible, so in [8], a slope based estimation approach was proposed.

Till now, the influences of the coil resistance and the induced voltage due to the rotor movement are neglected in the position estimation. The proposed approach in this paper takes them also into account and eliminates them. Thus, it should deliver better estimation performance. Details about the approach will be given in the following sections. Beginning with the simplified modelling in Section II, the basic idea of the proposed approach will be explained. Then, mechanisms to realize the idea will be given in Section III. This self-sensing technique will be applied to a real magnetic bearing, which has coupled control fluxes and permanent magnet excited bias fluxes. The modelling is quite different and has to be adapted. This will be explained in Section IV. Experimental results will be discussed in Section V. Conclusions and future work will be given in the last section.

II. MODELLING OF A SINGLE-AXIS ACTUATOR

To explain the proposed approach, the model of a single-axis actuator is shown in Fig. 1. We point out, that the proposed method is also valid for higher number of axes, as long as the magnetic paths of each electromagnet are independent from the other, which is the case for most hetero-polar magnetic bearings.

We define the origin of the *x*-axis in the middle between the two electromagnets and distinguish the electric and geometric quantities of different electromagnets with

subscripts $k = 1,2$. For simplification, we neglect eddy currents, flux leakage and edge flux effects and assume a sufficient high permeability $\mu_{\mathrm{Fe}} \to \infty$ of the laminated iron cores. Then, according to Faraday's law and to Ampere's law, we get the following basic equations:

$$\dot{\psi}_k + R_k i_k = u_k\,, \quad k = 1,2. \tag{1}$$

$$\psi_k = \frac{2\mu_0 A N^2 i_k}{\delta_k}\,, \quad k = 1,2. \tag{2}$$

In the above equations, ψ_k is the magnetic flux linkage of the electromagnet coil, R_k is the total coil resistance of each electromagnet, i_k is the coil current, u_k is the coil terminal voltage of the electromagnet, μ_0 is the permeability of free space, A is the area of each pole face, and N is the number of turns of one coil. So each electromagnet has a total number of turns of $2N$, and δ_k is the individual air gap width of each electromagnet. Additionally, we have the geometric constraints,

$$\delta_1 = X_0 - x\,, \tag{3}$$

$$\delta_2 = X_0 + x\,, \tag{4}$$

where X_0 is the nominal air gap width, and x is the position deviation. We apply the time derivative to both sides of (2) and get

$$\dot{\psi}_k = \frac{2\mu_0 A N^2}{\delta_k} \cdot \left(\dot{i}_k - \frac{i_k}{\delta_k} \dot{\delta}_k \right). \tag{5}$$

Both (1) and (5) are valid in the time domain. We put (1) into (5) and get

$$u_k - R_k i_k = \frac{2\mu_0 A N^2}{\delta_k} \cdot \left(\dot{i}_k - \frac{i_k}{\delta_k} \dot{\delta}_k \right). \tag{6}$$

If we use a two-level PWM (Pulse Width Modulation) amplifier, then the coil voltage u_k changes between U_{dc} and $-U_{\mathrm{dc}}$, where U_{dc} is the DC-link voltage of the PWM amplifier. Within one switching period, the following conditions,

$$u_k = -U_{\mathrm{dc}}\,, \tag{7}$$

during the negative switching interval, and

$$u_k = U_{\mathrm{dc}}\,, \tag{8}$$

during the positive switching interval, are given. In a digital control system, we can choose the control frequency equal to the PWM switching frequency f_{T}, which means that the fastest possible control is applied. Further, we apply two samples per PWM cycle. At these sample points, (7) and (8) are fulfilled respectively, as shown in Fig. 2. We consider the n^{th} PWM cycle and use the subscript α to represent the time interval T_α, when condition (7) is fulfilled, and β to represent the time interval T_β, when condition (8) is fulfilled: $T_\alpha + T_\beta = 1/f_{\mathrm{T}} = T_0$. Then we get two equations (9), (10), which are the discrete form of (6) during the negative and positive switching, respectively.

$$-U_{\mathrm{dc}} - R_k i_{k,n,\alpha} = \frac{2\mu_0 A N^2}{\delta_{k,n,\alpha}} \cdot \left(\dot{i}_{k,n,\alpha} - \frac{i_{k,n,\alpha}}{\delta_{k,n,\alpha}} \dot{\delta}_{k,n,\alpha} \right), \tag{9}$$

$$U_{\mathrm{dc}} - R_k i_{k,n,\beta} = \frac{2\mu_0 A N^2}{\delta_{k,n,\beta}} \cdot \left(\dot{i}_{k,n,\beta} - \frac{i_{k,n,\beta}}{\delta_{k,n,\beta}} \dot{\delta}_{k,n,\beta} \right). \tag{10}$$

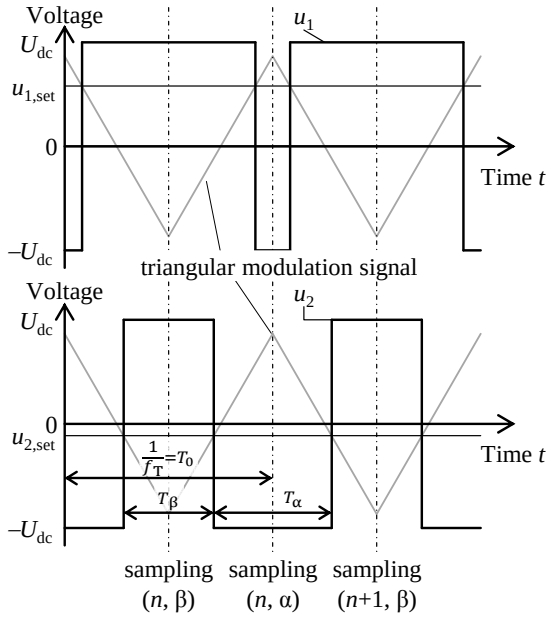

Fig. 2: Two-level PWM with double sampling per period

The time interval between the two samples (n, α) and (n, β) is half of the PWM period $1/(2f_{\mathrm{T}})$, which is sufficient small, so we could neglect the changes of the air gap width and the velocity of the positioned body. Then we have

$$\delta_{k,n,\alpha} \cong \delta_{k,n,\beta} = \delta_{k,n}\,, \tag{11}$$

$$\dot{\delta}_{k,n,\alpha} \cong \dot{\delta}_{k,n,\beta} = \dot{\delta}_{k,n}. \tag{12}$$

If the duty cycle of the n^{th} PWM cycle according to $T_\alpha = T_\beta$ is 50%, we can further assume that

$$i_{k,n,\alpha} \cong i_{k,n,\beta} = i_{k,n}\,. \tag{13}$$

With the simplifications of (11)-(13), we derive the following equation from (9) and (10),

$$\delta_{k,n} = -\frac{\mu_0 A N^2}{U_{\mathrm{dc}}} \dot{i}^*_{k,n}\,, \tag{14}$$

where

$$\dot{i}^*_{k,n} = \dot{i}_{k,n,\alpha} - \dot{i}_{k,n,\beta}\,. \tag{15}$$

Equation (14) estimates the air gap width of the corresponding electromagnet. In the modeling we do not neglect the influences of the coil resistance and the induced voltage due to the body movement, and we eliminate these influences with the double detection of the current slopes. Thus, (14) will deliver a more accurate position estimation. Further, if we exploit the geometric constraints of (3) and (4), then we can also eliminate the position offsets, consisting of the mechanical nominal air gap width and the additional equivalent air gap width due to the limited iron permeability $\mu_{\mathrm{Fe}} < \infty$! So from (3) and (4) we get

$$x_n = -\frac{\delta_{1,n} - \delta_{2,n}}{2}. \tag{16}$$

Finally, considering (14) and (16) we derive the final expression of the estimated position during the n^{th} cycle:

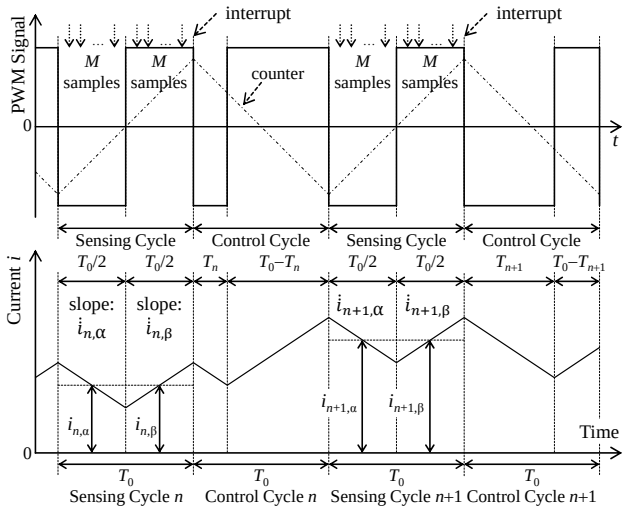

Fig. 3: PWM pattern with split sensing and control cycles (T_α=T_β=T_0/2)

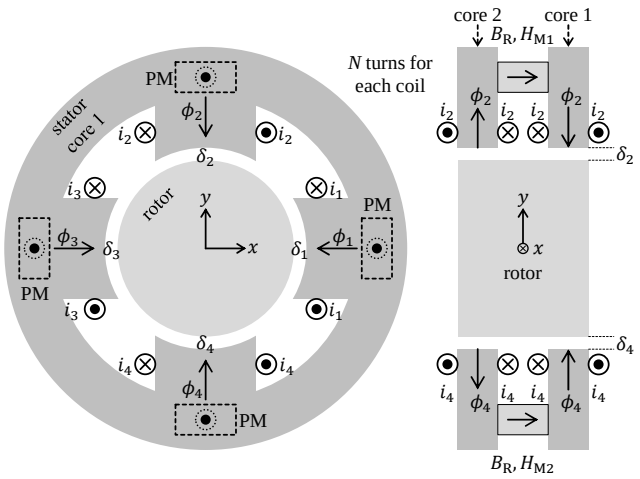

Fig. 4: Schematic representation of the used industrial magnetic bearing

$$x_n = \frac{\mu_0 A N^2}{2U_{\mathrm{dc}}} \cdot (\dot{i}^*_{1,n} - \dot{i}^*_{2,n})\,. \tag{17}$$

In the next section, implementation details will be explained, concerning the measurement of the current slopes and the mechanism to ensure the 50% PWM duty cycle for the position estimation.

III. Implementation of the Approach

The easiest way to measure the current slope is to use voltage transformers. With the current flowing through the primary coil of the transformer, the open terminal voltage of the secondary coil is proportional to the current slope, as described in [7]. This approach demands space for installing transformers, and it also increases the cost. So a modern way is to use high-speed A/D (Analogue to Digital) converters to sample several points within one switching state and calculate the current slope with the method of least squares [9-11].

As shown in the preliminary work in [12], the current slopes are calculated via software. The number of multiple samples, which determines the accuracy of the slope calculation, is therefore limited by the system data transfer rate. Considerable improvement was made in [13], in which the calculation is performed in the FPGA (Field Programmable Gate Array). Further, the introduction of splitting of the PWM pattern into a sensing cycle, which has a fixed duty cycle of 50%, and a control cycle, which has the variable duty cycle (T_0 –T_n)/T_0, (T_0 –T_{n+1})/T_0, … , for the current control, fits the requirement of (13) perfectly (Fig. 3). The duty cycle 50% gives zero change of the average current and does therefore not disturb the current control.

As shown in Fig. 3, we apply multiple sampling with M sample points twice during the sensing cycle. We show here only the slope calculation for negative switching as an example. For the n^{th} PWM cycle, we obtain with the M measured current values $i_{n,\alpha,0}$; … ; $i_{n,\alpha,M-1}$, measured at the time instants $t_{n,\alpha,0}$; … ; $t_{n,\alpha,M-1}$, the following current vector

$$\boldsymbol{i}_{n,\alpha} = \left[i_{n,\alpha,0}\; i_{n,\alpha,1}\; i_{n,\alpha,2}\; \cdots\; i_{n,\alpha,M-1}\right]^T, \tag{18}$$

with the corresponding time vector,

$$\boldsymbol{t}_{n,\alpha} = \left[t_{n,\alpha,0}\; t_{n,\alpha,1}\; t_{n,\alpha,2}\; \cdots\; t_{n,\alpha,M-1}\right]^T. \tag{19}$$

Then the current slope can be calculated using the method of least squares with

$$\dot{i}_{n,\alpha} = \frac{\sum_{j=0}^{M-1}\left(i_{n,\alpha,j} - \bar{i}_{n,\alpha}\right)\cdot\left(t_{n,\alpha,j} - \bar{t}_{n,\alpha}\right)}{\sum_{j=0}^{M-1}\left(t_{n,\alpha,j} - \bar{t}_{n,\alpha}\right)^2}\,, \tag{20}$$

where $\bar{i}_{n,\alpha}$ and $\bar{t}_{n,\alpha}$ are the mean value of the M components of the vectors (18) and (19). To simplify the calculation in FPGA, we choose a fixed time interval $T_{\mathrm{m.s.}}$ between neighbouring samples. Then the components of the time vector in (19) can be described by

$$t_{n,\alpha,j} = t_{n,\alpha,0} + j \cdot T_{\mathrm{m.s.}},\;\; j = 0, 1, 2, \cdots, M-1\,. \tag{21}$$

Considering (21), equation (20) becomes

$$\dot{i}_{n,\alpha} = \frac{\sum_{j=0}^{M-1}(2j - M + 1)\cdot i_{n,\alpha,j}}{\frac{1}{6}M\cdot(M^2-1)\cdot T_{\mathrm{m.s.}}}\,. \tag{22}$$

In the same way, the current slope of positive switching is given as

$$\dot{i}_{n,\beta} = \frac{\sum_{j=0}^{M-1}(2j - M + 1)\cdot i_{n,\beta,j}}{\frac{1}{6}M\cdot(M^2-1)\cdot T_{\mathrm{m.s.}}}\,. \tag{23}$$

With (22), (23) and (17), we determine the estimated position. The advantage is the simplicity of the system structure. From the hardware point of view, it is the same as a pure current control. Fewer hardware components mean increased reliability and more cost saving.

A compromise is made between the accuracy of the position estimation and the dynamic of the current control. Due to the additional sensing cycle, whose average voltage is zero but which lasts for T_0 like the control cycle (Fig. 3), the effective DC-link voltage for the current control is reduced to its half. Therefore, the current change rate, caused by sensing and control cycle, is slower than with a normal PWM pattern without additional sensing cycles. An approach to achieve the fastest possible current control under this limitation was also given in [13].

IV. APPLICATION TO A REAL MAGNETIC BEARING

The proposed self-sensing technique is applied to an industrial magnetic bearing, which has bias magnetic fluxes in axial direction, excited by permanent magnets, and coupled control fluxes in radial direction, excited by coils, as shown in Fig. 4. Therefore, due to the coupled magnetic paths of the two orthogonal *x* and *y* axes, the modelling is quite different to the one described in Section II.

We take the same assumption for the magnetic properties as in Section II ($\mu_{\mathrm{Fe}} \to \infty$) and define the quantities, shown in Fig. 4, as follows: For the subscripts $k = 1,2,3,4$, δ_k is the individual air gap width; ϕ_k is the total magnetic flux through the poles of the stator iron cores, which has opposite direction in stator core1 and core 2; i_k is the controlled coil current. Each coil has N turns, and the coils, which are located in the same position on stator core 1 and 2, are connected in series as a coil group. The voltage applied to each coil group is u_k; $H_{\mathrm{M},k}$ is the magnetic field strength in each permanent magnet in axial direction. Each magnet has the remanence B_{R}, the length in axial direction l_{M}, and the cross section area in the radial plane A_{M}. The cross section area of the poles is A_{P}. The permeabilities of the air and of the magnets are μ_0 and μ_{M}, respectively.

According to Ampere's law and Gauss's law for magnetism, we obtain 8 equations to describe the electro-magnetic properties of the given magnetic bearing. These equations are written in matrix form

$$\boldsymbol{A} \cdot \boldsymbol{s} = \boldsymbol{b} \tag{24}$$

with the matrix $\boldsymbol{A}$ defined as

$$\begin{bmatrix} a_0 & 0 & 0 & 0 & \delta_1 & 0 & 0 & 0 \\ 0 & a_0 & 0 & 0 & 0 & \delta_2 & 0 & 0 \\ 0 & 0 & a_0 & 0 & 0 & 0 & \delta_3 & 0 \\ 0 & 0 & 0 & a_0 & 0 & 0 & 0 & \delta_4 \\ 0 & 0 & 0 & 0 & -\delta_1 & \delta_2 & 0 & 0 \\ 0 & 0 & 0 & 0 & 0 & -\delta_2 & \delta_3 & 0 \\ 0 & 0 & 0 & 0 & 0 & 0 & -\delta_3 & \delta_4 \\ -a_1 & -a_1 & -a_1 & -a_1 & 1 & 1 & 1 & 1 \end{bmatrix}, \tag{25}$$

where $a_0 = 0.5\mu_0 A_{\mathrm{P}} l_{\mathrm{M}}$ and $a_1 = \mu_{\mathrm{M}} A_{\mathrm{M}}$. The vector of unknowns $\boldsymbol{s}$ is defined as

$$[H_{\mathrm{M},1} \quad H_{\mathrm{M},2} \quad H_{\mathrm{M},3} \quad H_{\mathrm{M},4} \quad \phi_1 \quad \phi_2 \quad \phi_3 \quad \phi_4]^{\mathrm{T}}. \tag{26}$$

The free term vector $\boldsymbol{b}$ is defined as

$$\begin{aligned} &\mu_0 A_{\mathrm{P}} N \cdot [i_1 \quad i_2 \quad -i_3 \quad -i_4 \\ &-i_1 + i_2 \quad -i_2 - i_3 \quad i_3 - i_4 \quad \frac{4B_{\mathrm{R}} A_{\mathrm{M}}}{\mu_0 A_{\mathrm{P}} N}]^{\mathrm{T}} \end{aligned} \tag{27}$$

with the positive direction of current flow as shown in Fig. 4.

We apply the time derivative to both sides of (24) and get

$$\dot{\boldsymbol{A}} \cdot \boldsymbol{s} + \boldsymbol{A} \cdot \dot{\boldsymbol{s}} = \dot{\boldsymbol{b}}. \tag{28}$$

Using the double slope detecting technique for the current signals, for the given n^{th} sensing cycle, we have

$$\dot{\boldsymbol{A}}_{n,\alpha} \cdot \boldsymbol{s}_{n,\alpha} + \boldsymbol{A}_{n,\alpha} \cdot \dot{\boldsymbol{s}}_{n,\alpha} = \dot{\boldsymbol{b}}_{n,\alpha}, \tag{29}$$

and

$$\dot{\boldsymbol{A}}_{n,\beta} \cdot \boldsymbol{s}_{n,\beta} + \boldsymbol{A}_{n,\beta} \cdot \dot{\boldsymbol{s}}_{n,\beta} = \dot{\boldsymbol{b}}_{n,\beta}. \tag{30}$$

The assumptions (11)-(13) are still valid, and we further assume due to the high switching frequency

$$H_{\mathrm{M},k,n,\alpha} \cong H_{\mathrm{M},k,n,\beta} = H_{\mathrm{M},k,n} \tag{31}$$

and

$$\phi_{k,n,\alpha} \cong \phi_{k,n,\beta} = \phi_{k,n}. \tag{32}$$

Then, (29) and (30) can be united to (33)

$$\boldsymbol{A}_n \cdot \left(\dot{\boldsymbol{s}}_{n,\alpha} - \dot{\boldsymbol{s}}_{n,\beta}\right) = \dot{\boldsymbol{b}}_{n,\alpha} - \dot{\boldsymbol{b}}_{n,\beta}. \tag{33}$$

We further define

$$\dot{H}^*_{\mathrm{M},k,n} = \dot{H}_{\mathrm{M},k,n,\alpha} - \dot{H}_{\mathrm{M},k,n,\beta} \tag{34}$$

and

$$\dot{\phi}^*_{k,n} = \dot{\phi}_{k,n,\alpha} - \dot{\phi}_{k,n,\beta}, \tag{35}$$

so we get

$$\boldsymbol{A}_n \cdot \dot{\boldsymbol{s}}^*_n = \dot{\boldsymbol{b}}^*_n. \tag{36}$$

According to Faraday's law, we have with the given arrow system of Fig. 4,

$$R_k i_k + 2N \frac{\mathrm{d}\phi_k}{\mathrm{d}t} = u_k, \quad \text{for } k = 1,2, \tag{37}$$

and

$$R_k i_k - 2N \frac{\mathrm{d}\phi_k}{\mathrm{d}t} = u_k, \quad \text{for } k = 3,4. \tag{38}$$

The coil terminal voltages during the α and β interval of the n^{th} sensing cycle are

$$u_{k,n,\alpha} = -U_{\mathrm{dc}} \text{ and } u_{k,n,\beta} = U_{\mathrm{dc}} \text{ for } k = 1,2,3,4. \tag{39}$$

Therefore, we get with (35), (37), (38) and (39)

$$\dot{\phi}^*_{k,n} = -\frac{U_{\mathrm{dc}}}{N}, \quad k = 1,2, \tag{40}$$

and

$$\dot{\phi}^*_{k,n} = \frac{U_{\mathrm{dc}}}{N}, \quad k = 3,4. \tag{41}$$

Now we construct a modified equation system, which takes the air gap widths $\delta_{k,n}$ as unknown variables instead of $\dot{\phi}^*_{k,n}$.

$$\widetilde{\boldsymbol{A}} \cdot \tilde{\boldsymbol{s}}_n = \widetilde{\boldsymbol{b}}_n \tag{42}$$

In (42) the matrix $\widetilde{\boldsymbol{A}}$ with constant coefficient is

$$\begin{bmatrix} a_0 & 0 & 0 & 0 & -a_2 & 0 & 0 & 0 \\ 0 & a_0 & 0 & 0 & 0 & -a_2 & 0 & 0 \\ 0 & 0 & a_0 & 0 & 0 & 0 & a_2 & 0 \\ 0 & 0 & 0 & a_0 & 0 & 0 & 0 & a_2 \\ 0 & 0 & 0 & 0 & a_2 & -a_2 & 0 & 0 \\ 0 & 0 & 0 & 0 & 0 & a_2 & a_2 & 0 \\ 0 & 0 & 0 & 0 & 0 & 0 & -a_2 & a_2 \\ a_1 & a_1 & a_1 & a_1 & 0 & 0 & 0 & 0 \end{bmatrix}, \tag{43}$$

where $a_2 = \frac{U_{\mathrm{dc}}}{N}$. The modified vector of unknowns $\tilde{\boldsymbol{s}}_n$ is

$$\begin{aligned} &[\dot{H}^*_{\mathrm{M},1,n} \quad \dot{H}^*_{\mathrm{M},2,n} \quad \dot{H}^*_{\mathrm{M},3,n} \quad \dot{H}^*_{\mathrm{M},4,n} \\ &\delta_{1,n} \quad \delta_{2,n} \quad \delta_{3,n} \quad \delta_{4,n}]^{\mathrm{T}} \end{aligned} \tag{44}$$

and the modified free term vector $\widetilde{\boldsymbol{b}}_n$ is

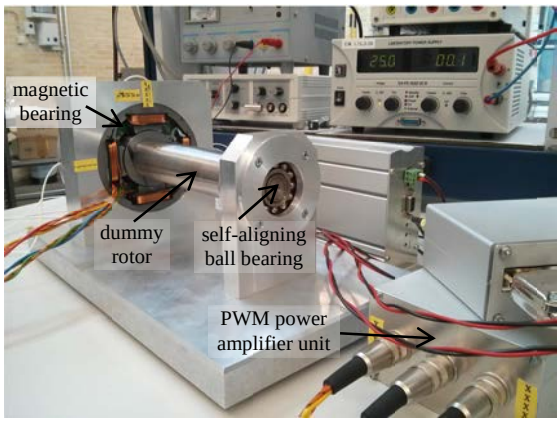

Fig. 5: Test bench of the self-sensing magnetic bearing

$$\mu_0 A_\mathrm{P} N \cdot \left[\dot{i}^*_{1,n} \quad \dot{i}^*_{2,n} \quad -\dot{i}^*_{3,n} \quad -\dot{i}^*_{4,n} \quad -\dot{i}^*_{1,n} + \dot{i}^*_{2,n} \quad -\dot{i}^*_{2,n} - \dot{i}^*_{3,n} \quad \dot{i}^*_{3,n} - \dot{i}^*_{4,n} \quad 0\right]^T . \tag{45}$$

We solve the linear equation system (42) for the air gap widths and get the four solutions

$$\delta_{k,n} = -\frac{\mu_0 A_\mathrm{P} N^2}{U_\mathrm{dc}} \dot{i}^*_{k,n} , \tag{46}$$

which have a similar expression as (14). Again, we apply the geometric constrains given as

$$x = -\frac{\delta_1 - \delta_3}{2} , \tag{47}$$

and

$$y = -\frac{\delta_2 - \delta_4}{2} . \tag{48}$$

Thus we finally obtain the expression of the position estimation as

$$x_n = \frac{\mu_0 A_\mathrm{P} N^2}{2 U_\mathrm{dc}} \cdot (\dot{i}^*_{1,n} - \dot{i}^*_{3,n}) \tag{49}$$

and

$$y_n = \frac{\mu_0 A_\mathrm{P} N^2}{2 U_\mathrm{dc}} \cdot (\dot{i}^*_{2,n} - \dot{i}^*_{4,n}) . \tag{50}$$

Equations (49) and (50) imply that only the axial fluxes, which are magnetically decoupled, are relevant for the position estimation. The coupled radial control fluxes do not seem to affect the algorithm. But we point out that due to the existing relative big leakage fluxes in axial direction, which are not included in the modelling, the position estimation is largely influenced by the coupled magnetic paths in the radial plane. The coupling trends to deform the estimated orbit in the radial plane into an ellipse form, as shown later in Section V.

V. Experimental results

We built a test bench to validate the proposed self-sensing technique. As shown in Fig. 5, the dummy rotor is supported by the magnetic bearing on the left side and by a self-aligning ball bearing on the right side. The used industrial magnetic bearing was equipped originally with a differential control winding, which is not suitable for the proposed self-sensing technique, because the current slopes of the individual coil groups are not accessible. Therefore, we spilt the connection between the coil groups to drive the four coil groups separately.

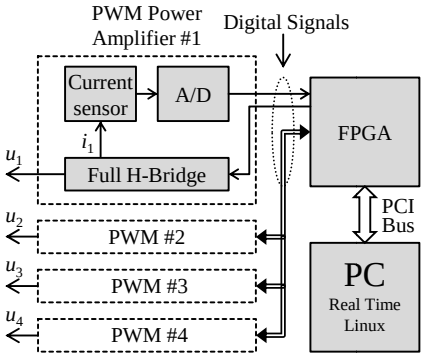

Fig. 6: Block diagram of the control system

Fig. 6 illustrates the structure of the control system. The PWM power amplifier unit is our own design, which has on-board current sensors and A/D converters, so that the currents are measured and digitized locally and transmitted digitally, which reduces the distortion of signal transmission, caused by electromagnetic interference of the excited coil groups. The full-bridge circuit and the A/D converter are driven by a FPGA board, which generates the PWM signals and synchronizes the multiple current sampling according to the timing illustrated in Fig. 3. The FPGA calculates additionally the current slope with (22) and (23). Thus, the FPGA serves as an interface between the magnetic bearing system and the control software, running on a PC under real time Linux.

The PWM switching frequency is $f_\mathrm{T} = 20$ kHz. The digital control works therefore on half of that frequency $f_\mathrm{T}/2 = 10$ kHz due to the timing with $2T_0$ of sensing and control cycle, as shown in Fig. 3. The present FPGA firmware features $M = 8$ as multiple current samples with $T_\mathrm{m.s.} = 2$ µs, which results in a 500 kHz sampling rate for the A/D converters. The used 12-bit A/D converter can be driven up to 1 MHz. So further improvements concerning the multiple sampling are possible. We also mounted position sensors on the magnetic bearing to get a reference signal for the position in comparison to the estimated position. A first evaluation concerning the static and transient performance of the position estimation was made with the enabled closed loop position control, using the measured position.

Fig. 7 shows the measured quasi-static performance of the position estimation. We control the rotor position so that it follows a circular orbit with a radius of about 75 µm around the central axis. It moves with a period of 5 s. We compare the estimated position with the measured position. The direct estimation output, using (49) and (50), is plotted in Fig. 7a and 7c. We obtained a different phase shift in *x*- and *y*-signals beside the general gain error for both axes: the estimated position signal of *x*-axis lags the measured position signal, while the estimated position signal of *y*-axis leads the measured position signal. This phase shift results in an elliptical deformation of the estimated orbit. As mentioned in Section IV, this deformation is caused by the coupled radial fluxes. This is a nature of the magnetic bearing, which means it could be corrected by an appropriate model. We choose the simple ellipse transformation for the correction and obtain the corrected position $(\tilde{x}_n, \tilde{y}_n)$ with the following equation

$$\begin{bmatrix} \tilde{x}_n \\ \tilde{y}_n \end{bmatrix} = \begin{bmatrix} g_1 & g_1 g_2 \\ g_1 g_2 & g_1 \end{bmatrix} \cdot \begin{bmatrix} x_n \\ y_n \end{bmatrix} , \tag{51}$$

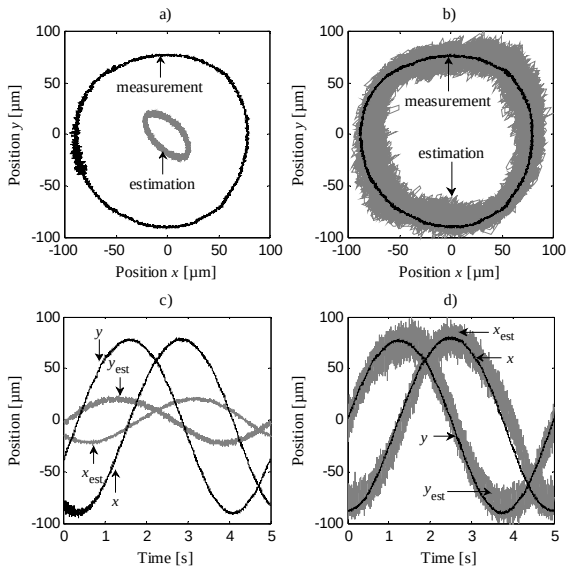

Fig. 7: Original and corrected position estimation vs. position measurement: a) Orbit of original position estimation, c) corresponding position curve of a), b) corected position estimation, d) corresponding position curve of b).

where g_1 is the common gain, which corrects the general gain error; and g_2 is the cross gain, which compensates the different phase shift of the position on the two orthogonal axes. After this correction (51), the estimated orbit now matches the measured orbit, as shown in Fig. 7b. The estimation and measurement are also in phase now, as shown in Fig. 7d. Due to the gain scaling, the noise band is generally amplified, which requires a further improvement concerning noise cancelling.

Fig. 8 shows the transient performance of the position estimation. The *x*-position of the rotor is kept at zero in the center. We give the *y*-axis position controller a step position command of 175 µm and record the measured and estimated position. The step response is given in Fig. 8c. A zoomed curve is plotted in Fig. 8d. During the step change of the real position on the *y*-axis, there is no noticeable delay of the estimated position, which means a very good dynamic performance. The estimated position on the *x*-axis remains unchanged, therefore, the cross coupling due to the coupled radial fluxes is completely eliminated.

VI. Conclusions and Future Work

A position estimation technique for self-sensing magnetic bearings is proposed in this paper. The derivation of the algorithm and the technical implementation is explained in detail. Experimental results show that the proposed technique also applies to existing industrial active magnetic bearings with coupled radial control fluxes and permanent magnet excited bias fluxes.

The future work will be focused on the improvement of signal processing to further reduce the noise level without loss of estimation dynamic. The position controller will be adapted for the estimated position as control feedback.

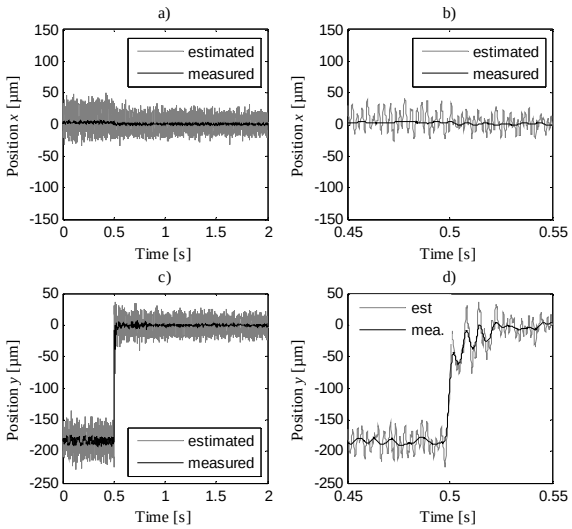

Fig.8: Estimation performance of step change of the real position in *y*- axis: a) Position of *x*-axis during step change of the position in *y*-axis, b) zoom of a), c) step change of the real position in *y*- axis, d) zoom of c).

References

[1] M. Brunet, U. Schroeder, Y. Tremaudant, "Active magnetic bearing with automatic detection of the position thereof," Patent WO2005103517 A1, 3 Nov., 2005.

[2] M. Morishita, H. Itoh, "The self-gap-detecting electromagnetic suspension system with robust stability against variation of levitation mass," in Proceedings of International Symposium on Power Electronics, Electrical Drives, Automation and Motion (SPEEDAM). 2006, pp. 1178-1183.

[3] K. Morita, T. Yoshida, K. Ohniwa, "Improvement of Sensing Characteristics of Self-Sensing Active Magnetic Bearings," Electrical Engineering in Japan, vol. 166, pp. 70-77, Jan. 2009.

[4] M. D. Noh, E. H. Maslen, "Self-sensing magnetic bearings using parameter estimation," IEEE Transactions on Instrumentation and Measurement, vol. 46, pp. 45-50, 1997.

[5] A. Schammass, R. Herzog, P. Bühler, et al., "New results for self-sensing active magnetic bearings using modulation approach," IEEE Transactions on Control Systems Technology, vol. 13, pp. 509-516, 2005.

[6] Y. Jung-Sik, K. Jang-Hwan, S. Seung-Ki, et al., "Sensorless position control of active magnetic bearings based on high frequency signal injection method," in Proceedings of Applied Power Electronics Conference and Exposition, Miami, USA, 2003, vol. 1, pp. 83-88.

[7] L. Lichuan, T. Shinshi, A. Shimokohbe, "State feedback control for active magnetic bearings based on current change rate alone," IEEE Transactions on Magnetics, vol. 40, pp. 3512-3517, 2004.

[8] A. C. Niemann, "Self-sensing Algorithms for Active Magnetic Bearings," Ph.D. Thesis, North-West University, 2008.

[9] J. Weigold, M. Braun, "Predictive Current Control Using Identification of Current Ripple," IEEE Transactions on Industrial Electronics, vol. 55, pp. 4346-4353, 2008.

[10] F. Becker, H. Ennadifi, M. Braun, "Straightforward current control - One step controller based on current slope detection," in Proceedings of 14th European Conference on Power Electronics and Applications (EPE), Birmingham, UK, 2011, 10 pages.

[11] A. Liske, P. Hofmeier, M. Braun, "Extended straightforward current control for permanent magnet synchronous machines," in Proceedings of 15th European Conference on Power Electronics and Applications (EPE), Lille, France, 2013, paper no. 0841, 10 pages.

[12] J. Wang, A. Binder, "Self-sensing magnetic bearings using multiple sampling of currents alone," in Proceedings of 15th European Conference on Power Electronics and Applications (EPE), Lille, France, 2013, paper no. 0210, 10 pages.

[13] J. Wang, A. Binder, "Current slope calculation in FPGA for sensorless control technique and associated slope based predictive precise current control," in Proceedings of IEEE International Symposium on Sensorless Control for Electrical Drives and Predictive Control of Electrical Drives and Power Electronics (SLED/PRECEDE) Munich, Germany, 2013, paper no. S3P1, 8 pages.